Journal of Materials Chemistry A

Accepted Manuscript

ROYAL SOCIETY OF CHEMISTRY

www.rsc.org/materialsA

Journal of Materials Chemistry A

PAPER

Template-Preparation of Three-Dimensional Molybdenum Phosphide Sponge as High Performance Electrode for Hydrogen Evolution

Received 00th January 20xx,
Accepted 00th January 20xx

DOI: 10.1039/x0xx00000x

www.rsc.org/

Chen Deng, [a] Fei Ding, [b] Xinyuan Li, [a] Yaofang Guo, [a] Wei Ni, [a] Huan Yan, [a] Kening Sun [a] and Yi-Ming Yan* [a]

Electrocatalysts play vital role in electrochemical water-splitting for hydrogen production. Here, we will report the preparation of a three-dimensional molybdenum phosphide (MoP) as a non-precious-metal electrocatalyst for hydrogen evolution reaction (HER) by using cheap sponge (polyurethane, PU) as sacrificed template. The obtained 3D MoP not only has high large surface area, but also possesses porous and channel-rich structure, which the sidewall of the pore is comprised of refined nanoparticles. The 3D MoP sponge was used as a bulky and bind-free HER electrode and exhibited excellent catalytic activity in acidic electrolyte (achieving 10 and 20 mA cm^{-2} at overpotential of 105 and 155 mV, respectively). In addition, this novel bulky HER electrode showed a relatively small Tafel slope of 126 mV dec^{-1}, a high exchange current density of 3.052 mA cm^{-2}, and the Faradaic efficiency of nearly 100 %. Furthermore, this bulky electrode revealed high tolerance and durability both in acid and basic condition, maintaining 96% and 93% of its initial catalytic activity after continuous tests for 60000s. Thus, our work paves a feasible way of fabricating cheap and highly efficient HER electrode in large-scale for electrochemical water-splitting technology.

1. Introduction

The increasing depletion of fossil fuels raises worldwide concerns on energy crisis and environment. In recent years, hydrogen has been vigorously pursued as clean and sustainable energy for replacing fossil fuels in 21st century.[1-2] Among different hydrogen production technologies, electrochemical water-splitting has attracted considerable attention due to its environmentally benign feature. Importantly, the required electricity for electrochemical water-splitting can be simply generated from renewable energy, such as wind, tide, and solar energy.[3] Electrocatalyst plays vital role in this process as it is highly necessary to drive hydrogen evolution reaction (HER) with high current density and low overpotential.[4] Although Pt based metals are regarded as the best HER electrocatalysts currently, the scarcity and high cost impede their wide usage. Therefore, the development of non-noble metal based electrocatalyst as an alternative for highly efficient HER is substantially important.[5-7]

Recently, Mo-based compounds were reported as efficient HER electrocatalysts, including MoS_2,[8-12] Mo_2C,[13-14] MoB,[15] $MoSe_2$,[16] $NiMoN_x$,[17] etc. Especially, MoS_2 has been prepared and investigated by many groups for its high HER activity. However, the activity of MoS_2 originates from the sulfur edges and the basal planes are inert.[18-19] As such, the application of MoS_2 is largely limited by its poor activity in bulky form or poor electrical conductivity of nanoparticles.[20-21] More recently, transition metal phosphides (TMPs) have been invoked numerous research efforts due to the prior works reported by Sun's group. TMPs were generally used as excellent catalysts for hydrodesulphurization (HDS) due to its promising property of reversible binding and dissociation of H_2 in HDS reaction.[22] Similarly, this unique property was adopted in HER and several TMPs, such as Ni_2P,[23] CoP,[24-26] and FeP[27-28] have been synthesized as efficient HER electrocatalysts. Molybdenum phosphide (MoP) is also known as an active HDS catalyst. Theoretical study of density functional theory has predicted that MoP can introduce a good "H delivery" system which attains nearly zero binding to H at a certain coverage.[3] Moreover, MoP exhibits high electrocatalytic activity even in bulky form without any conductive supports because of its metallic properties and good electrical conductivity.[29-30] To this end, MoP nanoparticles with interconnected network structure have been successfully synthesized, in which citric acid was found to play an important role in determining the electrocatalytic HER efficiency.[31] Also, Joshua et al. reported the synthesis of amorphous MoP nanoparticles and obtained

[a] Beijing Key Laboratory for Chemical Power Source and Green Catalysis, School of Chemical Engineering and Environment, Beijing Institute of Technology, Beijing, 100081, People's Republic of China. Email: bityanyiming@163.com
[b] National Key Laboratory of Power Sources, Tianjin Institute of Power Sources, Tianjin, 300381, People's Republic of China

†Electronic Supplementary Information (ESI) available: [Figure S1-14, Table S1-3, and Movie S1]. See DOI: 10.1039/x0xx00000x

high HER performance.[32] To engineer the MoP surface, Jaramillo group presented a sulfidation treatment of MoP, and the phosphosulfide surface (MoP|S) led to remarkable improvements in catalyst performance.[33] Despite these achievements, it is highly desirable to design and synthesize an efficient MoP based HER electrocatalyst with rational structure by considering following important factors: 1) As HER involves a gas evolution process at the surface of electrocatalyst, a three-dimensional (3D) porous structure of electrocatalyst contributes to attain high catalytic performance by facilitating the reaction kinetic in the channel-rich structure. 2) A large surface area of the electrocatalyst is beneficial either for increasing active sites, or for accelerating their interfacial electrocatalytic reactions by allowing rapid charge transfer in HER. 3) In contrast to traditional powder catalyst, a 3D and bulky electrode with great chemical stability is substantially preferable to be used as binder-free electrode for HER. It has advantages in practical applications by tailoring the electrode size to fit different electrochemical devices.

Keep these in mind, we are devoting to fabricate three-dimensional (3D), porous and bulky MoP electrode by using commercially available sponges as template for loading the in-situ synthesized MoP nanoparticles. Sponge (polyurethane, PU), a supermarket-available product, is low-cost and abundant resource. We have been previously reported the use of PU to prepare 3D carbon electrode materials for capacitive deionization.[34] In this work, sponges not only act as initial framework to mediate the growth of MoP nanoparticles by preventing the aggregation, but also help to form rich channel in the resulted structure. Remarkably, the obtained 3D MoP material exhibits promising mechanical stability as a bulky electrode for HER. A tailored MoP bulky electrode without any conductive support materials possesses highly efficiency for HER both in acidic and alkaline media. Thus, this work paves a viable way of fabricating cheap and high efficient HER electrode for large-scale hydrogen fuel production with electrochemical water splitting technology.

2. Experiment section

Materials synthesis and method

Ammonium molybdate tetrahydrate, ($(NH_4)_6Mo_7O_{24} \cdot 4H_2O$, Sinopharm Chemical Reagent, AR, ≥99.0%) and Ammonium hydrogen phosphate ($(NH_4)_2HPO_4$, Sinopharm Chemical Reagent, AR, ≥98.0%) were used as received without further purification. The sponges (polyurethane, PU), supermarket-available) were cut into cuboids with the size of approximately 20 mm×10 mm×5 mm after 30mins sonication in an absolute ethanol solution and deionized water, respectively. In a typical procedure, stoichiometric $(NH_4)_6Mo_7O_{24}•4H_2O$ and $(NH_4)_2HPO_4$ (Mo : P=1:1 in molar ratio) were dissolved in deionized water. The precursor solutions were aged in a water bath at 80 °C overnight. Then, the sponge cuboid was immersed into quantitative precursor solution to evacuate the bubbles and absorb the solution fully. After that, the sponges were dried in an oven at 80 °C. After evaporating water, the sponge cuboid was sintered for 3 h to prepare at ramping rate of 2 °C per min from room temperature to 500 °C. Subsequently, the obtained material was converted into bulky 3D MoP by temperature programmed reduction in H_2 at a flow rate of 150 sccm min^{-1}. During the TPR, the temperature procedure followed a heating rate of 5 °C per min from room temperature to 550 °C, then a heating rate of 1 °C per min to a certain temperature X (550, 600, 650, 700, 750 °C) as the final temperature and kept for 3h. After that, the MoP samples were passivated in 2 vol.% O_2/N_2 for 10h. Finally, a sponge-shaped MoP (3D MoP-X) was obtained. As control experiment, MoP without sponges (Bare MoP) was synthesized with the same procedure without using sponges as template.

Material Characterization

The morphology was characterized by a scanning electron microscope (SEM, QUANTA FEG 250) and high resolution transmission electron microscope (HRTEM, JEOLJEM 2010). Energy Dispersive Spectrometer (EDS) was carried out with a light element detector via the ZAF technique. The obtained products were characterized by X-ray diffraction (XRD, Rigaku Ultima IV, Cu Kα radiation, 40KV, 40 mA). X-ray photoelectron spectroscopy (XPS) was carried out on Physical Electronics 5400 ESCA. To account for charging effects, all spectra had been referenced to C (1s) at 284.4 eV. The specific surface area and pore size distribution were determined by N_2 adsorption-desorption measurements (Quantachrome Instrument ASIQM0VH002-5). GC measurements were conducted on GC-2014C with thermal conductivity detector and argon carrier gas.

Electrochemical Measurements

All the electrochemical tests were performed at room temperature in a standard three electrode system controlled by a CHI 660D electrochemistry workstation. Pt wire and saturated calomel electrode (SCE) were used as counter and reference electrodes, respectively. In all measurements, the SCE reference electrode was calibrated with respect to reversible hydrogen electrode (RHE). All the potentials reported in our work are expressed *vs.* the RHE. RHE calibration was performed experimentally according to reported method.[35] In 0.5 M H_2SO_4, E (RHE) = E (SCE) + 0.268 V; In 1.0 M KOH, E (RHE) = E (SCE) + 1.04 V. Linear sweep voltammetry (LSV) was conducted in electrolyte at room temperature with a sweep rate of 2 mV s^{-1}. Electrochemical impedance spectroscopy (EIS) measurements for the polarization of HER were also carried out in the frequency range of 100 kHz–0.1 Hz in a potentiostatic mode under the amplitude of 5 mV. All the electrochemical tests in this work were performed without IR compensation.

Preparation of working electrode

MoP modified GC electrode: The glass carbon electrode was polished and cleaned before use. All catalyst samples were ground into uniformity powder to prepare catalyst ink. Catalyst ink was typically made by dispersing 5 mg of catalyst

in a mixture of 495 µL ethanol and 495 µL DI-water. After adding 10 µL of 5 wt.% of Nafion solution (Alfa Aesar) and ultrasonication, 5 µL of the dispersion was drop-dried onto the glassy carbon electrode (0.0707 cm^2) to reach a catalyst loading of 0.35 mg cm^{-2}. Current density was normalized by the geometrical area of the working electrode.

3D MoP electrode: Every bulky sponge-shaped MoP (3D MoP) was fixed by silver wire at certain length to connect with external circuit. Compared with the current of 3D MoP, the current of silver wire was neglectable. Current density was normalized by the geometrical area of the 3D MoP electrode.

Results and discussion

Fig. 1 shows the optical photos of the pure sponge, the sponge saturated with precursors after calcination, and the resulted MoP sponge. As seen, the pure sponge turned to dark blue after saturated with precursors solution and calcination at 500 °C in air ambience for 3h. Subsequently, a black bulky sponge-shaped MoP (3D MoP) was obtained after reducing the dark blue sponge in a H_2 environment at various temperatures (550, 600, 650, 700 , 750 °C) for 3h.

Fig. 2a shows the scanning electron microscopy (SEM) images of 3D MoP-650, where rich channels and well-defined macro-pores can be clearly observed. Fig. 2b shows a SEM image at nanoparticles with a size of several nanometers. This structural feature can further verified by a SEM image of the fracture plane of the pore's sidewall, as shown in Fig. S1. Such a unique structure should be caused by the gas releasing during the pyrolysis treatment, as indicated by the following equation:

$$2(NH_4)_6Mo_7O_{24}\cdot 4H_2O+14(NH_4)_2HPO_4 \rightarrow 14MoO_3\cdot 7P_2O_5 + 40NH_3\uparrow + 35H_2O \quad (1)$$

$$14MoO_3\cdot 7P_2O_5+77H_2 \rightarrow 14MoP+77H_2O \quad (2)$$

Control experiment demonstrates that, without the loading of precursor solution, sponges could be entirely removed after the pyrolysis treatment at 500 °C (Fig. S2). Researchers have found that the polyurethanes are thermosetting polymers of which decomposition starts from 170℃, intensifies from 200° C and vaporizes at about 290° C. When the temperature reaches 300° C the polyurethane decomposition is practically completed.[36] In addition, bare MoP sample was prepared at 650 °C without using the sponge (PU) template. In order to confirm the existence of carbon on the surface of 3D MoP, Raman spectra of the 3D MoP-650 and bare MoP-650 were conducted. Both of samples showed the same Raman peaks and there was no carbon peaks observed in Fig. S3.

Fig. 1 Optical photos of the pure sponge, the sponge saturated precursors after calcination, and the black bulky sponge-shaped MoP (3D MoP).

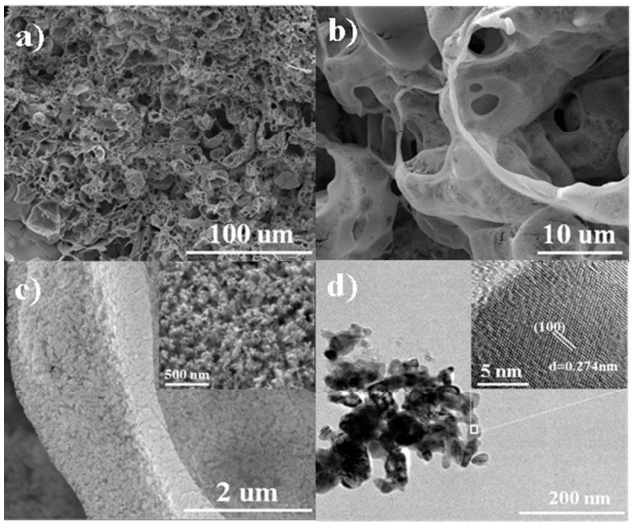

Fig. 2 (a) (b) and (c) show the SEM images of 3D MoP-650 at different magnification. (d) shows the TEM image of 3D MoP-650, the inset shows the HRTEM image.

Fig. S4 shows the SEM images of bare MoP sample, revealing that it consists of disordered and aggregated particles. Clearly, neither regular porous structure nor the refined sidewall was observed. This can be further verified by the nitrogen adsorption/desorption isotherms, as shown in Fig. S5. For 3D MoP-650 and bare MoP-650, the BET surface areas of 11.548 $m^2\ g^{-1}$ and 9.851 $m^2\ g^{-1}$, average pore sizes of 33.48 nm and 17.92 nm, and pore volumes of 0.085 $cm^3\ g^{-1}$ and 0.052 $cm^3\ g^{-1}$ were obtained, respectively. Table S1 gives the details of the BET higher magnification for different 3D samples, revealing that the 3D MoP-650 possesses an ideal loose structure which consists of plenty of mesopores and macropores beneficial for gas revolution and highest active surface areas which can accelerate the interfacial electrocatalytic reactions, resulting in effective charge transfer. With the increase of temperature, the aggregation of the particles increased, which can decrease the active surface area and pore size. Also, the thickness of the pore's sidewall of 3D MoP-650 can be estimated to be ca. 1 *um.* Interestedly, a close inspection on the structure of the sample, as shown in Fig. 2c and inset, displays that the sidewall of the pores is composed of refined results. As seen, the huge differences strongly suggest that sponge template plays critical role in determining the unique structure of the 3D MoP-650 sample. Sponges not only act as initial framework, but also can mediate the growth of particles and suppress the aggregation of MoP particles. As such, we anticipate that such a sponge-shaped 3D MoP with enriched porosity should own high active surface areas and help to accelerate their interfacial electrocatalytic reactions by allowing rapid charge transfer kinetics.

Fig. 2d gives the transmission electron microscopy (TEM) image of the 3D MoP-650 sample, displaying the nanoparticles-composed microstructure. Moreover, high-resolution TEM (HR-TEM) image, as the inset of Fig. 2d,

exhibits clear well-defined lattice fringes with a plane distance of 0.274 nm, which can be assigned to the typical (100) plane

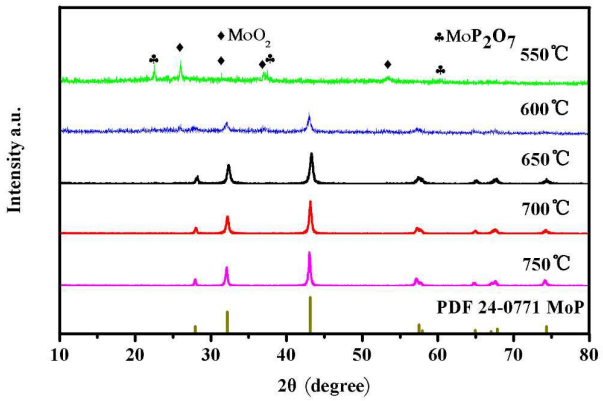

Fig. 3 XRD patterns of 3D MoP samples obtained at different reduction temperatures.

of molybdenum phosphide. Meanwhile, EDS measurements were conducted to reveal the mapping of Mo elemental and P elemental distribution at the sample surface (Fig. S6). We observed that both Mo and P elements were uniformly distributed in the obtained 3D MoP sample, suggesting that the as-prepared sponge-shaped sample is well-characterized MoP material.

To further confirm the compositional property, the X-ray diffraction (XRD) patterns of 3D MoP samples obtained at different reduction temperatures were presented. As shown in Fig. 3, the sample obtained at 550 °C (3D MoP-550) reveals characteristic peaks, which can be assigned to monoclinic molybdenum dioxide (JCPDS 32-0671) and cubic molybdenum phosphate (JCPDS 39-0026), respectively. Different from 3D MoP-550, other samples obtained at 600 °C, 650 °C, 700 °C, 750 °C show characteristic peaks at 27.9°, 31.2°, 43.1°, 57.5°, 58.0°, 65.0°, 67.0°, 67.9°, 74.3°, which should be assigned to (001), (100), (101), (110), (002), (111), (200), (102), and (201) plane of molybdenum phosphide (JCPDS 24-0771), respectively. Obviously, the XRD results demonstrate that typical molybdenum phosphide phase can't be formed at 550 °C reduction temperature in H_2 atmosphere. The crystalline degree of 3D MoP sample increases along with the reduction temperature. We found that only the reduction temperature is higher than 600 °C, the obtained 3D MoP sample turns to be crystallization. As seen, 3D MoP-650, 3D MoP-700 and 3D MoP-750 display well crystalline of WC-type hexagonal structure, while 3D MoP-600 shows poor crystallization. For comparison, Fig. S7 shows the XRD of bare MoP sample, which

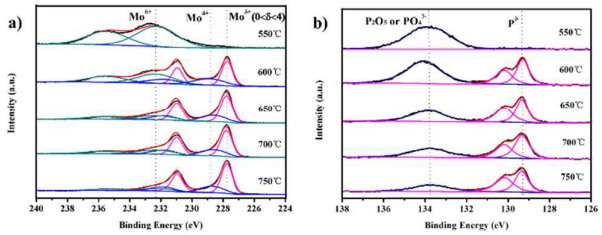

Fig. 4 X-ray photoelectron spectra (XPS) of the as-prepared 3D MoP samples: (a) Mo 3d region and (b) P 2p region.

is similar to that of 3D MoP 650.

To verify the different valence states of individual elements of 3D MoP samples, X-ray photoelectron spectroscopy (XPS) was adopted to characterize the binding energies of the Mo and P. Fig. 4a displays that the species have one or more oxidation states at the surface of bulky 3D MoP. The samples that obtained at the reduction temperature higher than 600 °C exhibit similar spectra with typical several doublets. Two doublets at ~235.5 eV/232.3 eV (Mo^{6+} $3d_{3/2}/3d_{5/2}$) and ~231.9 eV/228.8 eV (Mo^{4+} $3d_{3/2}/3d_{5/2}$) should be assigned to MoO_3 and MoO_2, respectively.[3,37] These species might be formed during the passivation treatment. According to previous studies, Mo 3d doublet at ~227.8 eV/231.0 eV indicative of $Mo^{\delta+}$ species ($0<\delta\leq4$) generally can be assigned to molybdenum element of molybdenum phosphide. [31,33, 38, 39] Noteworthy, the 3D MoP-550 exhibits only two characteristic peaks at 232.3 and 235.5 eV, which can be assigned to Mo^{6+}. XPS results show that no $Mo^{\delta+}$ species can be observed for 3D MoP-550, which is consistent with the XRD result. Also, for the profiles of P 2p, 3D MoP-550 sample only exhibits a peak at high binding energy of ~133.8 eV, which could be ascribed to PO_4^{3-} or P_2O_5.[39] In contrast, other samples display two peaks at 130.1 and 129.3 eV, which should be assigned to the binding energy (BE) of P $2p_{1/2}$ and P $2p_{3/2}$ (in Fig. 4b), respectively.[28,31] As seen, the BE of $Mo^{\delta+}$ species is higher than metallic Mo^0 (227.6 eV) ,thereby $Mo^{\delta+}$ has a strong binding affinity to H. Apart from this, the major P species with BE of 129.3 eV can be assigned to $P^{\delta-}$ bonded to Mo atom. It is known that $P^{\delta-}$ can induce a charge transfer from molybdenum to phosphorus, which can consequently downshift d-band center of molybdenum in 3D MoP and thereby decrease Mo-H binding energy. According to research before,[40] the strong molybdenum–hydrogen bonds on the surface may inhibit the hydrogen release from the active sites, but a simple phosphorization of molybdenum to form MoP introduces a good 'H delivery' system which can potentially modify the properties of the metal molybdenum, presenting excellent catalytic activity with a combination of experimental results and theoretical calculations.[3] Such an interaction benefits for the electrochemical desorption of H_{ads} and leads to a relatively moderate Mo–H binding strength, [31, 38, 41] therefore accelerating the hydrogen evolution reaction. Table S2 summaries the information derived from the XPS of 3D MoP prepared at different reduction temperature. As seen, the ratio of P : Mo decreases and the content of $P^{\delta-}$ and $Mo^{\delta+}$

increases along with the increase of reduction temperature. It has been reported that Mo serves as the active center of hydride-acceptor and P acts as the proton-acceptor center to facilitate the formation of Mo-hydride for subsequent hydrogen evolution via electrochemical desorption. Specifically, P sites can bond hydrogen at low coverage and desorb hydrogen at high coverage.[31, 42-45] Therefore, it is reasonable to conclude that there should be an optimized $Mo^{\delta+}$: $P^{\delta-}$ for achieving the best HER performance.

To further examine the catalytic activity of the 3D MoP samples, their HER performance was investigated in 0.5 M H_2SO_4 with a scan rate of 2 mV s^{-1}. In a typical three-electrode

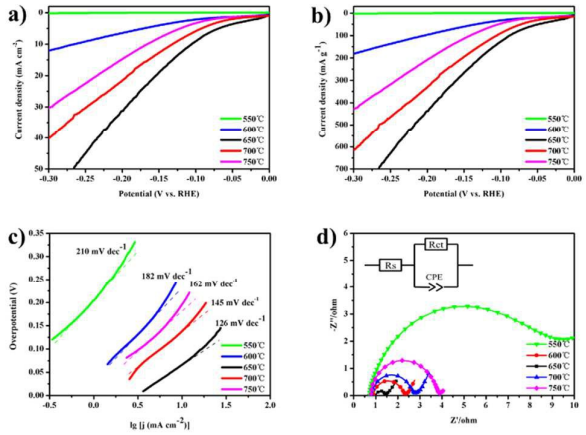

Fig. 5 Linear sweep voltammetry (LSV) curves of 3D MoP samples normalized by (a) the surface area and (b) total weight in 0.5 M H_2SO_4 at a scan rate of 2 mV s^{-1}. (c) The Tafel plots and the fitted slopes for 3D MoP samples. (d) The Nyquist plots of 3D MoP samples fitted with an equivalent circuit model.

system, the 3D bulky MoP sample was used directly as a working electrode without further treatment. The current of 3D MoP electrode was collected by using Ag wire as collector. Linear scanning voltammetry plots were recorded after an activation process at a scan rate of 100 mV s^{-1} from +0.1 V to -0.3V *vs.* RHE. We observed that the catalytic current became stable after 10 cycles activation. Fig. 5a shows the polarization curves for all the prepared 3D MoP samples. We noted that there is no platform at the beginning in the polarization curves, which is in agreement with the previously reported results [21, 46]. As seen, the 3D MoP-650 exhibits the highest HER efficiency among all the 3D MoP samples. The reduction current density increases rapidly along with negative potential scanning. The current density can approach 10 mA cm^{-2} and 20 mA cm^{-2} at overpotential of 105 mV and 155 mV, respectively. Meanwhile, it is clear that the HER activity of the samples exhibits a decreases tendency along with the increase of reduction temperature. In considering that the samples may has different weight, Fig. 5b presents particularly the measured current of polarization curves normalized by weight of samples, from which the tendency of HER activity for the samples is consistent with that observed in Fig. 5a. The results apparently suggest that proper reduction temperature for preparing the 3D MoP samples should determine the HER performance.

In general, the electrochemical evaluation of the HER activity for various electrocatalysts are represented by the

Table 1 Summary of the electrochemical parameters for all 3D MoP samples.

	550 ℃	600 ℃	650 ℃	700 ℃	750 ℃
Tafel slope b (mV dec-1)	210	182	126	145	162
Exchange current density (mA cm-2)	0.106	0.599	3.052	1.172	0.833
Charge-transfer Impedance (Ω)	10.5	1.4	0.5	1.9	3.0

kinetic values of constants *a* and *b*, which are calculated from the Tafel equation ($\eta = b \log j + a$). The constant *b*, called as Tafel slope which reflects the intrinsic property of catalysts, can be used to understand the reaction mechanism. The value of *b* is determined by the rate-limiting step of the HER. As reported [20], the Tafel slopes of 30, 40, and 120 mV dec^{-1} correlate with different rate determining steps of HER. Another important parameter for judging the inherent electrocatalytic activities of electrocatalysts is the exchange current density (j_0), which represents as a significant kinetic factor of the electrochemical reaction rate at equilibrium state. It reflects how rapidly the electrochemical reaction can occur at an elelctrocatalyst. [48] The value of j_0 can deduced from the linear area of Tafel plot, corresponding to the intercept at the overpotential $\eta = 0$. Fig. 5c displays the Tafel plot derived from the fitted polarization curves of the 3D MoP samples. The Tafel slopes are 162 , 145, 126, 182, and 210 mV dec^{-1} for 3D MoP samples of 750 ℃, 700 ℃, 650 ℃, 600℃, and 550 ℃, respectively. We noted that the Tafel slopes for all 3D MoP samples are much larger than the values for other reported MoP [3, 30-32] (40–70 mA dec^{-1}). It suggests that the HER mechanism for 3D MoP samples might be quite different from typical Heyrovsky reaction or Tafel reaction. [46] In fact, the value of Tafel slope can be influenced by several factors, including the reaction pathway and the adsorption conditions of the active site.[27, 47] In spite that more detailed work are needed to illustrate this, we propose that the unique 3D structure full of channels and porosity might affect the observed Tafel slope of the MoP samples. Molybdenum phosphide is a good conductor of electricity compared with other semi-conductor and displays a metallic character shown by density functional theory (DFT) analyses. However, as the oxide layer produced during preparation and storage on the surface, the conductivity of 3D MoP would be affected overall which would decrease its conductivity. Without other conductive materials or additional electrode to support, 3D MoP which is massive presented higher Tafel than the Tafel slope on MoP modified GCE electrode due to their large oxide surface and unique stereostructure. Among all the samples, 3D MoP-650 exhibits the smallest Tafel slope of 126 mV dec^{-1} and the largest exchange current density of 3.052 mA cm^{-2}. To understand this, electrochemical impedance spectroscopy

(EIS) technique was applied to examine the 3D MoPs in acidic conditions. The Nyquist plots of the samples and the corresponding electrical equivalent circuit diagram are given in Fig. 5d. As shown, 3D MoP-650 exhibits much lower charge-transfer impedance (*Rct*) of ~ 0.5 Ω comparing to other samples. Table 1 lists the obtained electrochemical parameters, in terms of Tafel slope, impedance and exchange current density, for all 3D MoP samples. The observed promising performance for 3D MoP-650 should be ascribed to the following reasons: 1) The significantly small impedance affords markedly faster HER kinetics. 2) The high surface area and porous structure offer more exposed active sites and enable the rapid diffusion of species during the reactions. 3) Good crystalline and appropriate $Mo^{\delta+}$: $P^{\delta-}$ might contribute to the high activity.

Next, it is essentially necessary to verify the advantages of the bulky 3D structure of MoP in HER. For this purpose, 3D MoP-650 was grinded into powder (called P-MoP) and modified on glassy carbon electrode (GCE). For comparison, bare GCE, commercial Pt/C (5 wt.% Pt/XC-72) and Bare MoP reduced at 650 °C were also studied. As shown in Fig. S8a, bare GCE almost shows no HER activity, while Bare MoP exhibits a higher activity than bare GCE. In contrast, P-MoP modified on GCE has relatively high activity toward HER with onset overpotential of 60 mV (*vs.* RHE). Also, it can approach a current density of 2 and 10 mA cm^{-2} at overpotential of 115 mV and 191 mV, respectively. Fig. S8b shows the Tafel plots derived from the polarization measurements. As seen, P-MoP shows a Tafel slope of 56 mV dec^{-1}, which is similar to the values reported by other groups. [3,31] The TOF per active site for the P-MoP is calculated to be 0.90 s^{-1} (vs. 0.14 s^{-1} of bare MoP) at η = 0 mVs^{-1}. Therefore, our templated synthetic method provides a facile and green route to prepare high-performance HER catalyst. Obviously, P-MoP has better HER performance than Bare MoP, which can be probably explained by the fact that P-MoP possesses the refined nanoparticles assembled structure and should expose more active site. Specifically, we found that 3D bulky MoP electrode possesses much higher HER activity than P-MoP modified electrode. It indicates that the 3D and bulky structure has superiority towards HER. Two reasons might be responsible for the observed results. On one hand, P-MoP modified electrode was prepared by using polymer binder to immobilize electrocatalyst, which correspondingly increases the resistance, [49] blocks some active sites and inhibits gas diffusion, thereby deteriorating the overall catalytic activity of the electrode. [50] On the other hand, the 3D MoP sponge electrode offers large surface area, rich inter connected channels, and ideal porosity, which are extremely beneficial for catalytical reaction and gas evolution. We also compare the performance of 3D MoP sample with other Mo-based HER electrocatalysts. As shown in Table S3, the as-prepared 3D MoP outperforms most of the reported HER electrocatalsyts.

Apart from the electrochemical activity, stability is another vital factor for judging the electrocatalyst. To this end, long-term stability of 3D MoP electrode was investigated in 0.5 M H_2SO_4 by maintaining overpotential of 110 mV. Fig. 6 shows that the reduction current density remained at around 11 mA cm^{-2} even after 60000s continuous operation, where almost 96% of the initial current was kept. For a sharp comparison, only 78% and 82% of initial current density were maintained of P-MoP electrode and Pt/C, respectively (Fig. S9). These results demonstrate that 3D bulky electrode has superior stability in a long-term electrochemical process over traditional catalyst powder modified electrode. To verify the composition of the sample, we further characterized the XRD and XPS of 3D MoP-650 sample after long-term stability test. As illustrated in Fig. S10, the XRD peaks of the sample before and after long term test remained the same, indicating the same crystallographic structure. In Fig. S11, we found that the constituent of 3D MoP-650 sample remained stable and there is no much distinction after testing except that the relative intensities of

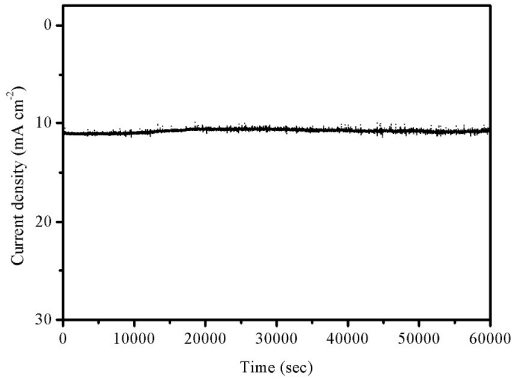

Fig. 6 Time dependence of catalytic current density during electrolysis for 3D MoP-650 in 0.5 M H_2SO_4 at overpotential of 90 mV.

its Mo $3d_{5/2}$ and P $2p_{3/2}$ peaks with higher binding energies were lower than before which could be contributed to active hydrogen species H possessing high reduction abilities to reduce molybdenum and phosphorus oxides during test. However, the intensity of molybdenum and phosphorus oxides increased after long-term storage again, which could be attributed to the long-term exposure to air during practical operation. We have supplemented the SEM of the sample after long-term electrochemical test as shown in Fig. S12. After electrochemical test for 60000s, the 3D porous structure of the sample didn't change (Fig. S12a). However, the surface of the sample became rougher, which can be attributed to the generation of the bubbles during the HER process. During the experiments for P-MoP and Pt/C, we observed that the freshly formed hydrogen bubbles were strongly absorbed to the electrode surface and hardly detached until that they grow into large size. Such a feature is undesirable as the adhesions of bubbles not only lower the gas evolution rate, but also increase the risk of the catalyst corrosion. It has been proved that porous structure and rough surface contribute to suppress gas bubble adhesion, and enhance electrode stability

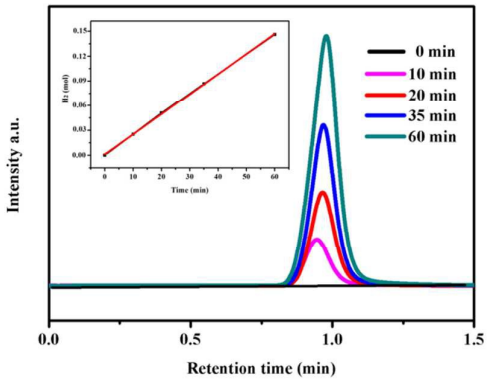

Fig. 7 The GC chromatograph of H_2 gas production obtained with 3D MoP-650 under electrolysis at -0.2 V (*vs.* RHE) for 1h. The inset shows the volume of hydrogen and the testing time.

by accelerating the detaching process of the hydrogen bubbles. [51] To clarify this, Fig. S13 gives the pictures of 3D MoP-650 electrode in the solution before and during HER. As seen, the small sized H_2 bubbles were found to evolve from the bulky electrode. Moreover, Movie S1 clearly displays the working process for hydrogen production at the 3D MoP-650 operated from +0.05 V to -0.35 V. As a result, it strongly demonstrates that the 3D MoP sponge electrode is highly efficient and favorable for hydrogen production using in electrochemical water-splitting. Although Pt-based catalysts have been widely studied towards HER, very few catalysts show high performance under both acidic and basic conditions. Recently, some solid-state catalysts have emerged as efficient HER catalysts which can operate in both acidic and basic solutions.[3,15, 52] In this work, we also investigated the activity of 3D MoP under basic condition. As shown in Fig. S14a, the activity of 3D MoP-650 in 1 M KOH is surprisingly as high as that in acidic solutions. Remarkably, the durability of 3D MoP electrode in 1 M KOH was also tested (Fig. S14b). Nearly 93% of the initial current was maintained, indicating that 3D MoP electrode owns superior tolerance to solution pH. Nevertheless, we noted that further studies are necessary to understand the mechanism of 3D MoP in strong acid and alkaline solution.

Finally, we used the gas chromatography (GC) to detect the gas product at the 3D-MoP electrode. As shown in Fig. 7, only H_2 was detected without any other product, implying that the electrode works well for hydrogen evolution. Furthermore, the amount of collected H_2 shows linear dependence along with the increasing time of electrolysis. By taking into account of the charge passed through the cell, the faradaic efficiency for HER at 3D-MoP electrode was calculated to be nearly 100 %. It substantially suggests that the bulky 3D MoP sponge can serve as high performance electrode for electrochemical hydrogen production. Importantly, the unique structure feature enables 3D MoP sponge high applicability by tailoring the size and coupling with the electrochemical devices in practical applications.

Conclusions

In summary, we have reported a simple synthetic strategy for the preparation of bulky 3D MoP electrode for HER by using the low-cost and commercial sponge as scarified template. The prepared MoP materials showed unique sponge-shaped structure consisting of rich channels and pores, which are beneficial for gas evolution. Significantly, the sidewall of the pores was comprised of well-defined nanoparticles, endowing the materials with high surface area and much exposed active sites. The 3D MoP-650 afforded relatively small Tafel slope of 126 mV dec^{-1}, a high exchange current density of 3.052 mA cm^{-2}, and a Faradaic efficiency of nearly 100 % in acidic electrolyte. Only 105 mV of overpotential was needed to achieve 10 mA cm^{-2} current density. In addition, this novel bulky HER electrode showed high tolerance and promising durability both in acid and basic condition. Importantly, the unique structural features and compositional properties endow the 3D MoP sponge advantages of easy coupling with different electrochemical devices by tailoring the electrode size without adding any binder agent or conductive support. Therefore, this work essentially offers a cheap, viable and scale-up strategy of preparing high efficient HER electrocatalyst for electrochemical water-splitting technology.

Acknowledgements

Financial supports from the Ministry of Science and Technology (2012DFR40240), National Natural Science Foundation of China (Grant nos. 21175012), and the Chinese Ministry of Education (Project of New Century Excellent Talents in University: NCET-10-0048) are gratefully acknowledged.

Notes and references

1 J. A. Turner, *Science*, 2004, **305**, 972-974.
2 N. S. Lewis, *Science*, 2007, **315**, 798-801.
3 P. Xiao, M. A. Sk, L. Thia, X. Ge, R. J. Lim, J. Y. Wang, K. H. Lima and X. Wang, *Energy Environ. Sci.*, 2014, **7**, 2624-2629.
4 M. G. Walter, E. L. Warren, J. R. McKone, S. W. Boettcher, Q. Mi, E. A. Santori and N. S. Lewis, *Chem. Rev.*, 2010, **110**, 6446-6473.
5 Y. Hara, N. Minami, H. Matsumoto and H. Itagaki, *Appl. Catal. A*, 2007, **332**, 289-296.
6 H. B. Gray, *Nat. Chem.*, 2009, **1**, 7-7.
7 D. V. Esposito, S. T. Hunt, A. L. Stottlemyer, K. D. Dobson, B. E. McCandless, R. W. Birkmire and J. G. Chen, *Angew. Chem. Int. Ed.*, 2010, **49**, 9859-9862.
8 T. F. Jaramillo, K. P. Jorgensen, J. Bonde, J. H. Nielsen, S. Horch and I. Chorkendorff, *Science*, 2007, **317**, 100-102.
9 Y. Hou, B. Zhang, Z. H. Wen, S. M. Cui, X. R. Guo, Z. He and J. H. Chen, *J. Mater. Chem. A*, 2014, **2**, 13795-13800.
10 J. Kibsgaard, Z. Chen, B. N. Reinecke and T. F. Jaramillo, *Nat. Mater.*, 2012, **11**, 963-969.
11 Z. Chen, D. Cummins, B. N. Reinecke, E. Clark, M. K. Sunkara and T. F. Jaramillo, *Nano Lett.*, 2011, **11**, 4168-4175.
12 J. Deng, H. Li, J. Xiao, Y. Tu, D. Deng, H. Yang, H. Tian, J. Li, P. Ren and X. Bao, *Energy Environ. Sci.*, 2015, **8**, 1594-1601.

13 W. Chen, C. Wang, K. Sasaki, N. Marinkovic, W. Xu, J. T. Muckerman, Y. Zhu and R. R. Adzic, *Energy Environ. Sci.*, 2013, **6**, 943-951.
14 L. Liao, S. Wang, J. Xiao, X. Bian, Y. Zhang, M. D. Scanlon, X. Hu, Y. Tang, B. Liu and H. H. Girault, *Energy Environ. Sci.*, 2014, **7**, 387-392.
15 H. Vrubel and X. Hu, *Angew. Chem. Int. Ed.*, 2012, **51**, 12703 - 12706.
16 D. Kong, H. Wang, J. J. Cha, M. Past , K. J. Koski, J. Yao and Y. Cui, *Nano Lett.*, 2013, **13**, 1341-1347.
17 W. F. Chen, K. Sasaki, C. Ma, A. I. Frenkel, N. Marinkovic, J. T. Muckerman, Y. Zhu and R. R. Adzic, *Angew. Chem. Int. Ed.*, 2012, **51**, 6131-6135.
18 J. Yang and H. S. Shin, *J. Mater. Chem. A*, 2014, **2**, 5979-5985.
19 J. Bonde, P. G. Moses, T. F. Jaramillo, J. K. Nørskov, I. Chorkendorff, *Faraday Discuss*, 2008, **140**, 219-231.
20 Y. Li, H. Wang, L. Xie, Y. Liang, G. Hong and H. Dai, *J. Am. Chem. Soc.*, 2011, **133**, 7296-7299.
21 Y. H. Chang , C. T. Lin , T. Y. Chen , C. L. Hsu , Y. H. Lee ,W. Zhang , K. H. Wei and L.J. Li, *Adv. Mater.*, 2013, **25**, 756-760.
22 P. Liu and J. A. Rodriguez, *J. Am. Chem. Soc.*, 2005, **127**, 14871-14878.
23 Y. Bai, H. Zhang, X. Li, L. Liu, H. Xu, H. Qiu and Yu Wang, *Nanoscale*, 2015, **7**, 1446-1453.
24 J. Tian, Q. Liu, A. M. Asiri and X. Sun, *J. Am. Chem. Soc.*, 2014, **136**, 7587-7590.
25 Z. Pu, Q. Liu, P. Jiang, A. M. Asiri, A. Y. Obaid and X. Sun, *Chem. Mater.*, 2014, **26**, 4326-4329.
26 E. J. Popczun, C. G. Read, C. W. Roske, N. S. Lewis and R. E. Schaak, *Angew. Chem. Int. Ed.*, 2014, **53**, 5427-5430.
27 Y. Xu, R. Wu, J. Zhang, Y. Shi and B. Zhang, *Chem. Commun.*, 2013, **49**, 6656-6658.
28 P. Jiang, Q. Liu, Y. Liang, J. Tian, A. M. Asiri and X. Sun, *Angew. Chem. Int. Ed.*, 2014, **53**, 12855-12859.
29 S. T. Oyama, *J. Catal.*, 2003, **216**, 343-352.
30 X. Chen, D. Wang, Z. Wang, P. Zhou, Z. Wu and F. Jiang, *Chem. Commun.*, 2014, **50**, 11683-11685.
31 Z. Xing, Q. Liu, A. M. Asiri and X. Sun, *Adv. Mater.*, 2014, **26**, 5702-5707.
32 J. M. McEnaney, J. C. Crompton, J. F. Callejas, E. J. Popczun, A. J. Biacchi, N. S. Lewis and R. E. Schaak, *Chem. Mater.*, 2014, **26**, 4826-4831.
33 J. Kibsgaard and T. F. Jaramillo, *Angew. Chem.*, 2014, **126**, 1-6.
34 Z. Y. Yang, L.J Jin, G. Q. Lu, Q. Q. Xiao, Y. X. Zhang, L. Jing, X. X. Zhang, Y. M. Yan and K. N. Sun, *Adv. Funct. Mater.*, 2014, **24**, 3917-3925.
35 Y. F. Xu, M. R. Gao, Y. R. Zheng, J. Jiang and S. H. Yu, *Angew. Chem. Int. Ed.*, 2013, **52**, 8546 -8550.
36 R. Bilbao, J. F. Mastral, J. Ceamanos and M. E. Aldea, *J. Anal. Appl. Pyrol.s*, 1996, **37**, 69–82.
37 X. Zhao, M. Cao, B. Liu, Y. Tian and C. Hu, *J. Mater. Chem.*, 2012, **22**, 13334-13340.
38 D. C. Phillips, S. J. Sawhill, R. Self and M. E. Bussell, *J. Catal.*, 2002, **207**, 266-273.
39 J. Bai, X. Li, A. Wang, R. Prins and Y. Wang, *J. Catal.*, 2012, **287**, 161-169.
40 Q. Yue, Y. Wan, Z. Sun, X. Wu, Y. Yuan and P. Du, *J. Mater. Chem. A*, 2015, **3**, 16941–16947.
41 R. Wang, K. J. Smith, *Appl. Catal. A-Gen.*, 2009, **363**, 18-25.
42 A. B. Laursen, S. Kegnaes, S. Dahl and I. Chorkendorff, *Energy Environ. Sci.*, 2012, **5**, 5577-5591.
43 W. Zhang, J. Hong, J. Zheng, Z. Huang, J. Zhou and R. Xu, *J. Am. Chem. Soc.*, 2011, **133**, 20680-20683.
44 A. D. Wilson, R. H. Newell, M. J. McNevin, J. T. Muckerman, M. R. Dubois and D. L. Dubois, *J. Am. Chem. Soc.*, 2006, **128**, 358-366.
45 B. E. Barton, T. B. Rauchfuss, *J. Am. Chem. Soc.*, 2010, **132**, 14877-14885.
46 Y. H. Chang, F. Y. Wu, T. Y. Chen, C. L. Hsu, C. H. Chen, F. Wiryo, K. H. Wei, C. Y. Chiang and L. J. Li, *Small*, 2014, **10**, 895-900.
47 B. E. Conway, B. V. Tilak, *Electrochim. Acta*, 2002, **47**, 3571-3594.
48 Y. Yan, B. Xia, Z. Xu and X. Wang, *ACS Catal.*, 2014, **4**, 1693-1705.
49 Y. Luo, J. Jiang, W. Zhou, H. Yang, J. Luo, X. Qi, H. Zhang, D. Y. W. Yu, C. M. Li and T. Yu, *J. Mater. Chem.*, 2012, **22**, 8634-8640.
50 J. D. Roy-Mayhew, G. Boschloo, A. Hagfeldt and I. A. Aksay, *ACS Appl. Mater. Interfaces*, 2012, **4**, 2794-2800.
51 Z. Lu, W. Zhu, X. Yu, H. Zhang, Y. Li, X. Sun, X. Wang, H. Wang, J. Wang, J. Luo, X. Lei and L. Jiang, *Adv. Mater.*, 2014, **26**, 2683-2687.
52 X. Zou, X. Huang, A. Goswami, R. Silva, B. R. Sathe, E. Mikmeková and T. Asefa, *Angew. Chem. Int. Ed.*, 2014, **53**, 4372-4376.

Table of content

Template-Preparation of Three-Dimensional Molybdenum Phosphide Sponge as High Performance Electrode for Hydrogen Evolution

Chen Deng, [a] *Fei Ding,* [b] *Xinyuan Li,* [a] *Yaofang Guo,* [a] *Wei Ni,* [a] *Huan Yan,* [a] *Kening Sun* [a] *and Yi-Ming Yan** [a]

Keywords: molybdenum phosphide, HER, sponge, three-dimensional electrode, bind-free

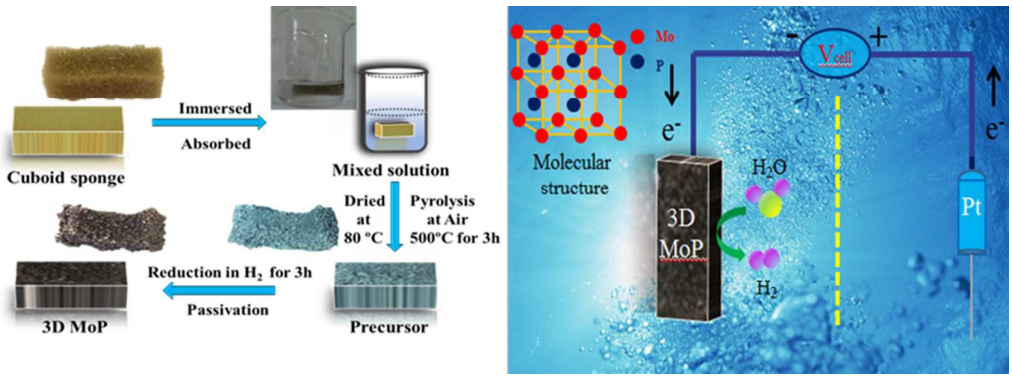

A sponge-shaped three-dimensional MoP (3D MoP) electrocalatalyst is prepared and used as a bind-free electrode for HER, exhibiting promising catalytic activity.